Optically detected magnetic resonance of nitrogen-vacancy centers in diamond under weak laser excitation

Yong-Hong Yu,[1,2] Rui-Zhi Zhang,[1,2] Yue Xu,[1,2] Xiu-Qi Chen,[1,2] Huijie Zheng,[1,3,*] Quan Li,[4] Ren-Bao Liu,[4] Xin-Yu Pan,[1,3,5] Dmitry Budker,[6,7,8] and Gang-Qin Liu[1,3,5,†]

[1] *Beijing National Laboratory for Condensed Matter Physics, Institute of Physics, Chinese Academy of Sciences, Beijing 100190, China*

[2] *School of Physical Sciences, University of Chinese Academy of Sciences, Beijing 100049, China*

[3] *Songshan Lake Materials Laboratory, Dongguan, Guangdong 523808, China*

[4] *Department of Physics, Centre for Quantum Coherence, and The Hong Kong Institute of Quantum Information Science and Technology, The Chinese University of Hong Kong, New Territories, Hong Kong, China*

[5] *CAS Center of Excellence in Topological Quantum Computation, Beijing 100190, China*

[6] *Johannes Gutenberg-Universität Mainz, Mainz 55128, Germany*

[7] *Helmholtz-Institut, GSI Helmholtzzentrum für Schwerionenforschung, Mainz 55128, Germany*

[8] *Department of Physics, University of California, Berkeley, California 94720, USA*

(Received 28 August 2023; revised 27 February 2024; accepted 26 March 2024; published 26 April 2024)

As promising quantum sensors, nitrogen-vacancy (N-V) centers in diamond have been widely used in frontier studies in condensed-matter physics, material science, and life sciences. In practical applications, weak laser excitation is favorable as it reduces the side effects of laser irradiation, such as phototoxicity and heating. Here we report a combined theoretical and experimental study of (near) zero-field optically detected magnetic resonance (ODMR) of N-V-center ensembles under weak 532-nm laser excitation. In this region, both the width and splitting of the ODMR spectra decrease with increasing laser power. This power dependence is reproduced with a model that accounts for the laser-induced charge neutralization of N-V^-–N^+ pairs, which alters the local electric field environment. These results are useful for the understanding and development of N-V-based quantum sensing in light-sensitive applications.

DOI: 10.1103/PhysRevApplied.21.044051

I. INTRODUCTION

Spin defects in solids with an optical interface are among the leading platforms for quantum information science and quantum sensing. Among the many spin defects, the negatively charged nitrogen-vacancy (N-V^-) center in diamond stands out, exhibiting excellent spin coherence, bright photoluminescence, and large contrast of magnetic resonance signal [1]. For quantum sensing applications, these features bring remarkable sensitivity in detecting magnetic field [2–4], temperature [5,6], pressure, and other physical quantities [7,8]. At the same time, the atomic structure of an N-V center enables spatial resolution down to the nanoscale, and the ultrastable diamond structure is compatible with complex biochemical environments [9], even under extreme conditions, such as megabar pressures [10] or sub-Kelvin temperatures [11].

Laser excitation provides an efficient and convenient way to establish the polarization and readout of N-V electron spin, and has been widely used in N-V-based quantum techniques. However, in practical applications, laser excitation also brings undesirable effects. For example, phototoxicity is a key issue when studying living cells with fluorescent probes. Recent experiments have shown that even weak laser excitation could bring adverse effects to living cells [12,13]. Another side effect is light-induced sample heating, which is a serious obstacle for temperature-sensitive applications, such as the characterization of superconducting films or magnetic films with low transition temperatures [11,14–17], and temperature-controlled cell division during early embryogenesis [18].

A straightforward strategy to reduce laser-induced side effects is to use laser beams of sufficiently low intensity, but the intrinsic properties of N-V centers, including charge, spin, and optical properties, have been poorly studied under weak excitation. Jensen *et al.* reported light narrowing of the microwave power-broadened magnetic resonance signals of N-V centers under a small magnetic field, which was attributed to the light-induced reduction of the N-V spin relaxation time (T_1) [19]. Under optical pumping, the charge conversion of an N-V center (between

*Corresponding author: hjzheng@iphy.ac.cn
†Corresponding author: gqliu@iphy.ac.cn

N-V^- and N-V^0) is inevitable [20], and the randomly distributed charges, either from N-V centers or from nearby charge traps, creating internal electric fields around the N-V center [21]. Therefore, it is necessary to consider both the charge and spin degrees of freedom together and revisit the magnetic resonance of N-V centers under weak laser excitation. Recently, Manson *et al.* made a step in this direction and showed that the charge conversion of N-V^-–N^+ pairs is crucial for understanding the optical properties of N-V centers in diamond [22].

In this paper, we report a combined theoretical and experimental study on optically detected magnetic resonance (ODMR) of N-V centers under weak green laser (532-nm) excitation. Ensembles of N-V centers in nanodiamonds, microdiamonds, and bulk diamonds are studied. When the excitation laser power is much smaller (one or more orders of magnitude) than the optical saturation power, both the width and the splitting of ODMR spectra decrease as the optical intensity increases. This phenomenon is well interpreted with a model that takes into account the laser-induced charge neutralization of N-V^-–N^+ pairs in diamond.

II. RESULTS

A nitrogen-vacancy center is formed by a substitutional nitrogen atom and a nearby vacancy in the diamond lattice. It has two common charge states, N-V^- and N-V^0, with featured zero-phonon lines (ZPL) at 637 and 574 nm, respectively. The negatively charged N-V^- center is a natural spin qubit, it exhibits spin-dependent optical transitions that enable high-fidelity spin polarization and readout through optical methods. In contrast, it is more difficult to initialize and read out the spin state of an N-V^0 center (a spin-half system) [23]. Laser excitation induces charge conversion of N-V centers (between N-V^- and N-V^0), either by two- or one-photon ionization processes [20,24].

The main finding of this work is that the internal electric field around an N-V center is mainly determined by its nearby substitutional nitrogen atoms and can be modified by the excitation light, with the effect becoming more pronounced in the weak excitation regime. It is generally believed that the extra electron of an N-V^- center is captured from a nearby defect, for example, another nitrogen atom (P1 center) [22]. In this scenario, the negatively charged N-V^- center is often accompanied by a positively charged N^+. Although the diamond is electrically neutral overall, these randomly distributed charges (N-V^-, N^+, and other charge traps) lead to internal electric fields at the N-V positions [21]. Under laser excitation, the charge distribution and the associated internal electric field in the diamond lattice are altered, leading to observable changes in the optical and spin properties of the remaining N-V centers, as illustrated in Fig. 1(a).

We start by measuring the PL spectra of N-V centers under weak laser excitation. Nanodiamonds (NDs) with ensemble N-V centers are deposited on strontium titanate (or alumina) substrates and measured in a home-built confocal microscopy. The average size of NDs is about 100 nm, with an N-V concentration of about 3 ppm (Adámas Nanotechnologies). Figure 1(b) shows typical PL spectra of these NDs, measured at 8.4 K. The ZPLs of N-V^- (637 nm) and N-V^0 (574 nm) are well resolved. The relative amplitude of the two peaks shows pronounced dependence on the laser intensity. We adopt a method described by Shinei *et al.* to quantitatively estimate the ratio of remaining N-V^- centers at different laser intensities. The method takes into account the integration of the ZPL peaks, the Huang Rhys factor, and the lifetime of the excited state of both centers (N-V^- and N-V^0) [25]. As summarized in Fig. 1(d), laser intensity plays a role in determining the charge state of N-V centers in diamond, and weak excitation leads to more N-V^- centers [26]. Note that a similar phenomenon has been reported [26,27].

Next, we show that the laser-induced charge conversion also strongly affects the N-V magnetic resonance signal. ODMR spectra of N-V^- centers in diamond are obtained by monitoring the photoluminescence intensity while simultaneously scanning the frequency of the applied microwave pulses [1]. Figure 1(b) shows typical ODMR spectra of the same nanodiamond, exhibiting a two-dip feature at 2.87 GHz, the value of zero-field splitting of N-V centers at cryogenic temperatures. The resonant frequencies and widths are extracted by numerical fitting, and their power dependence is summarized in Fig. 1(d). In the weak excitation region, both the splitting and the width of the ODMR spectra decrease with laser power. We measured several different NDs, all of which show a similar power dependence (see Supplemental Material [28] for extended data) (see also Refs. [29–38] therein).

To check whether this observation is a general effect, three other batches of diamond samples are measured. First, ODMR spectra of ensemble N-V centers in microdiamonds (MDs) and a bulk diamond (S5), with similar nitrogen concentration (about 200 ppm), are shown in Figs. 2(a) and 2(b). The laser power dependence of ODMR splitting and width of these spectra, as summarized in Figs. 2(d) and 2(e), are similar to that of NDs, indicating that particle size is not a key factor for this effect.

Secondly, ODMR spectra of another bulk diamond (E6-2) with similar N-V concentration but more dilute N concentration (approximately 14 ppm) are measured, as shown in Fig. 2(c). In this measurement, pairs of coils were used to compensate for the background magnetic field in the laboratory. The main feature of these ODMR spectra is the hyperfine splitting caused by the host ^{14}N nuclear spins. Numerical fitting considering the internal electric field and hyperfine coupling is used to extract the ODMR

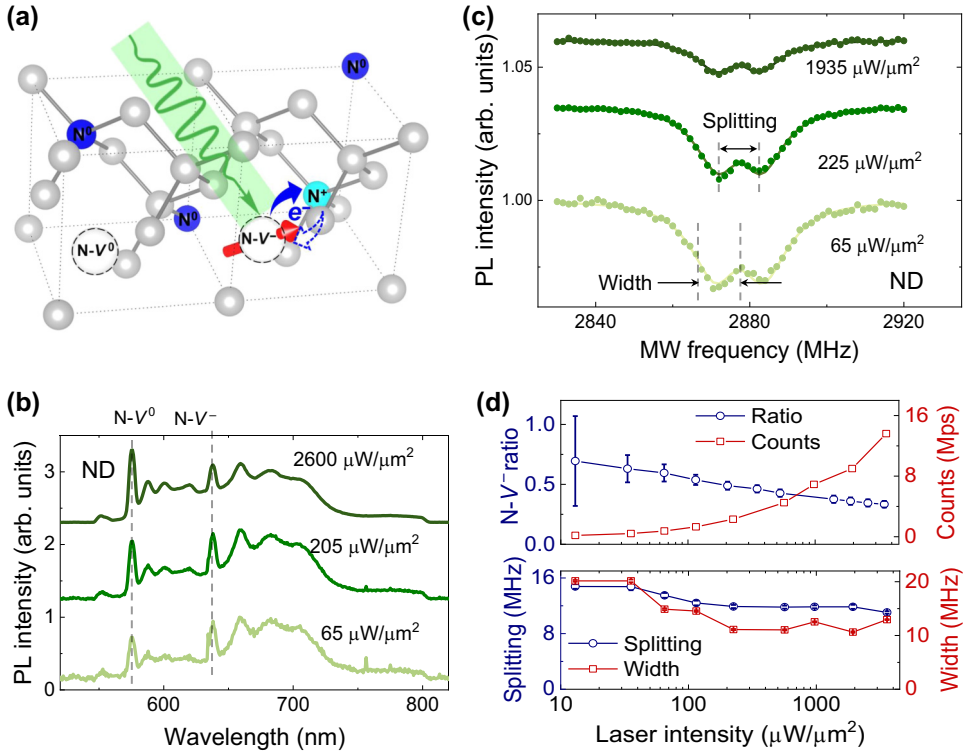

FIG. 1. Laser-induced charge neutralization of N-V^-–N^+ pairs in diamond. (a) Schematic representation of the N-V^-–N^+ model. After the absorption of photons, N-V^-–N^+ pairs could change into N-V^0–N^0 pairs, which leads to a more dilute charge distribution in the diamond lattice and thus smaller internal electric fields acting on the remaining N-V centers. (b) PL spectra of a nanodiamond measured at 8.4 K. The curves are vertically offset for better visibility. (c) Zero-field ODMR spectra of the same nanodiamond, measured at different laser powers. (d) Laser power dependence of the N-V^- ratio and photon count (upper pane), the splitting, and width of the ODMR spectra (lower pane).

splitting and width. Both parameters decrease slightly with increasing laser power, as can be seen in the inset of Fig. 2(f).

Summarizing, key features of N-V ODMR spectra have unambiguous laser power dependence. The effect is more pronounced in the weak excitation region and is closely related to the nitrogen concentration of the diamond sample.

To understand these results quantitatively, we adapt the N-V^-–N^+ pair model [22] developed by Manson *et al.* and pay special attention to the internal electric field around N-V centers [21]. Key points of this model are as follows: (1) N-V and N defects are randomly distributed in the diamond lattice. (2) Each N-V center captures an electron from one of its nearby N atoms and forms an N-V^-–N^+ pair. (3) The resonance frequencies of each N-V center are modified by its local internal electric field. (4) Upon laser excitation, some of the N-V^-–N^+ pairs are charge neutralized, resulting in more dilute charge density and smaller internal electric fields for the remaining N-V^- centers.

For simplicity, we assume that an N-V center always pairs with its nearby N atoms. The local electric field at the N-V position contains two parts: the electric field from its paired N^+ ion (E_N) and the dipole fields (E_{dipole}) from all other N-V^-–N^+ pairs. For the nano- and microdiamond samples, the N concentration (approximately 200 ppm) is much larger than the N-V concentration (3 ppm), so the distance between different pairs is much larger than the distance between the two point charges (N-V^- and its nearby N^+). As a result, the E_N component dominates the internal electric field and the E_{dipole} term can be ignored. Under these conditions, the splitting and the width of ODMR spectra of ensemble N-V centers can be related to the N concentration (see Supplemental Material [28] for detailed derivation):

$$S_{ODMR} \approx 0.42\ \rho_N^{\frac{2}{3}}\ \mathrm{MHz/ppm^{\frac{2}{3}}},$$
$$W_{ODMR} \approx 0.31\ \rho_N^{\frac{2}{3}}\ \mathrm{MHz/ppm^{\frac{2}{3}}}, \quad (1)$$

where ρ_N is the concentration of the N atoms (in ppm). It is clear that a dense N distribution leads to a large splitting and broadening feature to the ODMR spectra. When the N-V and N concentrations are of the same order of magnitude, for example, in the E6-2 sample, both the E_N and E_{dipole} terms should be taken into account, but the nitrogen

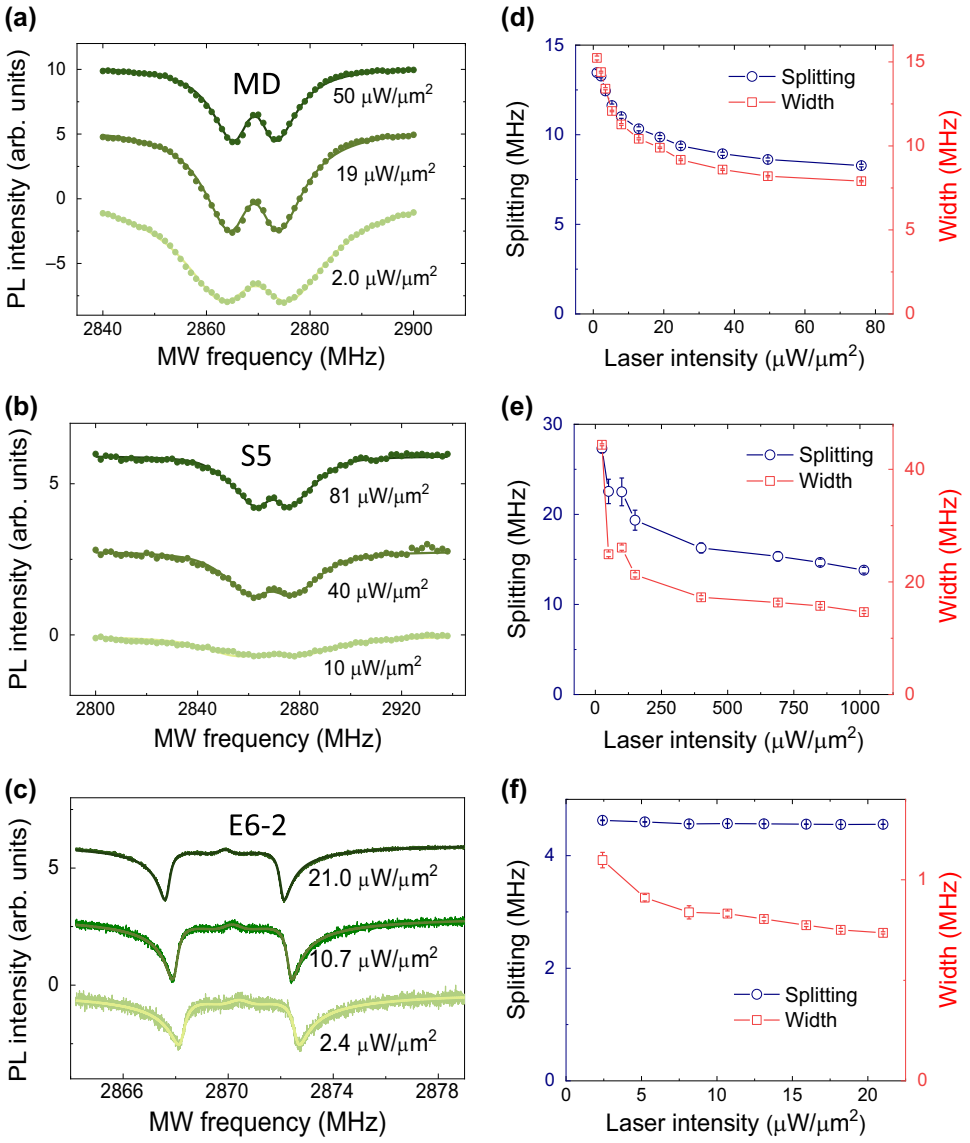

FIG. 2. (a)–(c) ODMR spectra of N-V centers in microdiamonds (MDs), and bulk diamonds (S5 and E6-2) under weak laser excitation, see Table I for detailed sample information. The spectra of MD and sample S5 are measured under Earth's magnetic field. The spectra of sample E6-2 are measured under zero magnetic field. (d)–(f) Laser power dependence of the ODMR splitting and width for the (d) MD sample, (e) S5 sample, and (f) E6-2 sample.

concentration dependence of ODMR parameters is similar to the former case.

With the model in hand, we now use numerical simulations to investigate the effects of nitrogen density and laser-induced charge neutralization on the key features of ODMR spectra. N-V centers and N atoms are randomly placed in a sphere of 100-nm diameter, and the total number of N-V centers (and N atoms) is chosen to match the known defect concentrations. The positions of the ith N-V center and the j th N atom are denoted as $\{\vec{r}_i\}$ and $\{\vec{r}_j\}$, respectively. The electric field on the ith N-V^- center is

$$\vec{E}^i = \frac{-e}{4\pi\epsilon_0\epsilon_r}\left[\sum_{k\neq i}\frac{\hat{r}_{ki}}{r_{ki}^2} - \sum_j \frac{\hat{r}_{ji}}{r_{ji}^2}\right], \tag{2}$$

where ϵ_0 is the vacuum permittivity, $\epsilon_r = 5.7$ is the relative permittivity of diamond [30], and r_{ki} and r_{ji} are

TABLE I. Details of diamond samples used in this work.

Sample	Size	[N]	[N-V]
ND	∼100 nm	∼200 ppm	∼3 ppm
MD	∼1 μm	∼200 ppm	∼3 ppm
S5	$3 \times 3 \times 0.5$ mm^3	∼200 ppm	5–40 ppm
E6-2	$3 \times 3 \times 0.7$ mm^3	14 ppm	∼3 ppm

the distances from the kth N-V^- and jth N^+ to the N-V position, $\hat{r}_{ki}$ and $\hat{r}_{ji}$ are the corresponding unit vectors.

This electric field can be decomposed into parallel (E^i_z) and perpendicular ($E^i_{\{x,y\}}$) components relative to the N-V axis, and it couples to the N-V electron spin through $\Pi^i_{\{x,y\}} = d_\perp E^i_{\{x,y\}}$ and $\Pi^i_z = d_\parallel E^i_z$, with susceptibilities $\{d_\parallel, d_\perp\} = \{0.35, 17\}$ Hz cm/V [21,29]. Specifically, the axial component of the electric field shifts the resonant frequency of the N-V center, and the transverse component splits the resonant peaks. It is worth noting that the coefficient of the transverse component ($d_\perp$) is much larger than that of the axial component ($d_\parallel$), resulting in the two-dip feature of the ensemble N-V ODMR spectra [21].

The N-V spin Hamiltonian under the electric field is [8]

$$H_i = \left(D_{gs} + \Pi^i_z\right) S^2_z + \Pi^i_x \left(S^2_y - S^2_x\right) + \Pi^i_y \left(S_x S_y + S_y S_x\right), \tag{3}$$

where the $D_{\rm gs} = (2\pi) \times 2.87$ GHz is the zero-filed splitting at room temperature, and S is the N-V spin operator. We have ignored the hyperfine coupling to the host ^{14}N and nearby ^{13}C nuclear spins in the calculation, as they are constant and do not change under laser excitation. After the diagonalization of the Hamiltonian, the eigenvalues of each N-V center and the corresponding resonant frequencies are obtained. For a given defect concentration, the calculation has been repeated 10^5 times, and the resonant frequencies of all N-V centers are taken into account to obtain their statistical features.

Figure 3(a) presents the probability distribution of the N-V resonant frequency under different N concentrations. Although intrinsic spin dephasing and technical broadening factors (e.g., microwave power broadening) have not been taken into account, these numerical spectra capture the key features of the experimentally measured ODMR spectra. The numerical results confirm that a dense N distribution leads to a large splitting and broadening to the ODMR spectra, as summarized in Fig. 3(b). The numerical results also fit well with the theoretical formula of Eq. (1). As an application of this result, one can use the ODMR splitting and width under zero field to estimate the nitrogen concentration of unknown diamond samples if the light illumination is sufficiently well characterized. From a diamond material growth and N-V^- center generation point of view, as a large nitrogen concentration is a prerequisite for dense N-V centers, it is preferred to maximize the efficiency of nitrogen to N-V center conversion and leave few nitrogen impurities (P1 centers) in the diamond lattice.

In order to directly compare the numerical results with the experimental ODMR spectra, we incorporate the effects of N-V spin dephasing and microwave power broadening in the numerical simulation. Considering the effect of microwave driving, the ODMR spectra are broadened by a factor proportional to $\Omega_R^2/(\Omega_R^2 + (2\pi\,\Delta)^2)$, where Ω_R is the Rabi frequency and Δ is the detuning of the driving microwave. With the following parameters: N-V^- concentration [N-V^-] = 3 ppm, nitrogen concentration [N] = 200 ppm, $1/T_2^* = 2$ MHz, and $\Omega_R = 2\pi \times 4$ MHz, the simulation results are in good agreement with the experimental ODMR spectra, as shown in Figs. 4(a) and 4(b). Details can be found in the Supplemental Material [28].

We then consider the role of laser excitation in determining the key feature of ODMR spectra in the weak excitation region. First-principles calculations suggest that the energy required for the N-V^0 + N^0 $\Rightarrow$ N-V^-–N^+ reaction is always negative [39]. Therefore, N-V^-–N^+ pairs are stable in the dark. Under laser excitation, however, the reverse process can take place, and part of the N-V^-–N^+ pairs are charge neutralized. In our measured samples, this most likely takes place through a one-photon process [40], as weak laser excitation is sufficient to induce this effect. The

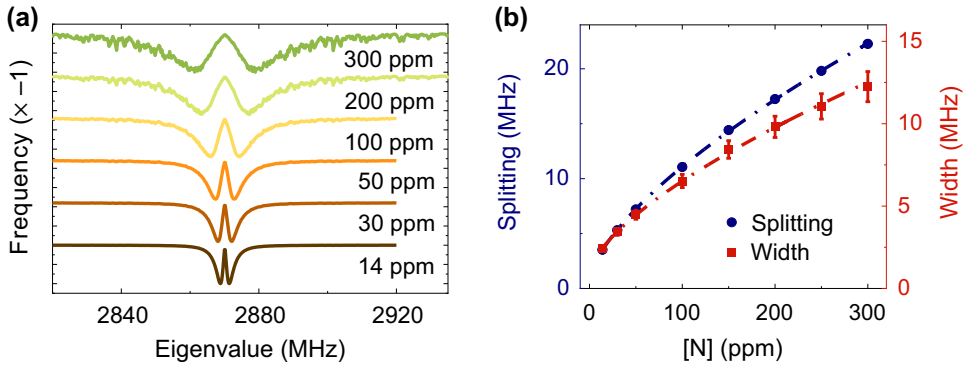

FIG. 3. Numerical results on nitrogen concentration. (a) The probability distribution of N-V resonant frequency under different nitrogen concentrations ([N-V^-] = 3 ppm). (b) Splitting and width of the numerical spectra as a function of the nitrogen concentration. The dashed lines are fitting results with Eq. (1). Note that spin relaxation, spin dephasing, and other technical broadening factors (e.g., microwave power broadening) are not considered in this simulation.

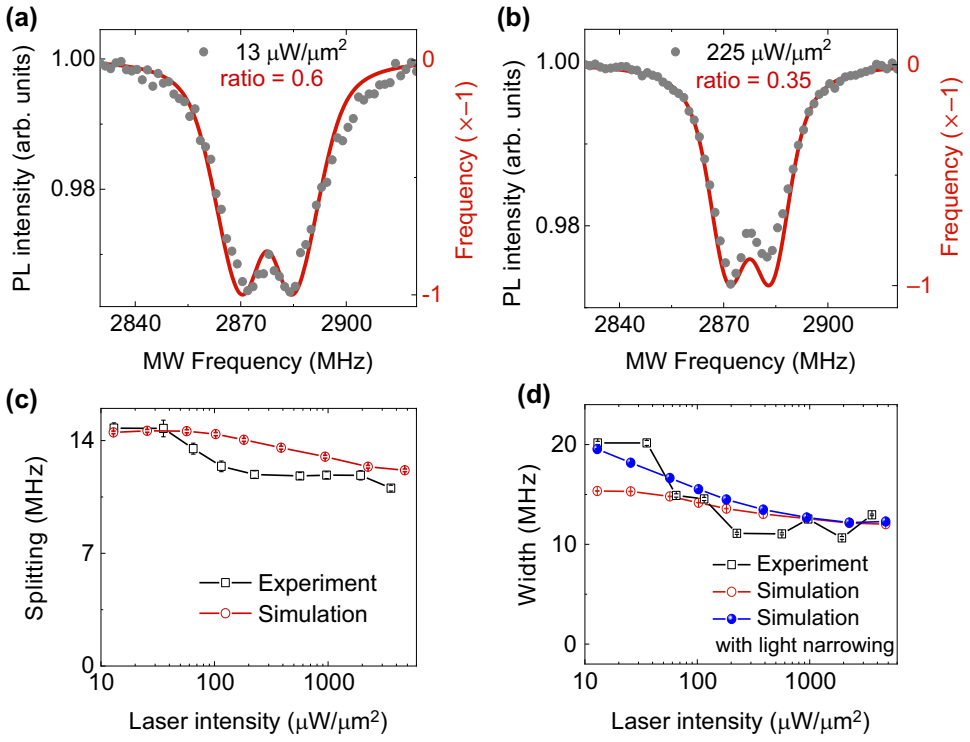

FIG. 4. Comparison between numerical and experimental results. (a),(b) Experimentally measured (gray dots) and numerically simulated (red lines) ODMR spectra of an ND at various laser powers. For the numerical simulation, each laser power is converted into the corresponding N-V^- ratio for the simulation. The parameters for the numerical simulation are [N] = 200 ppm, [N-V^-] = 3 ppm, $1/T_2^\star = 2$ MHz and $\Omega_R = 2\pi \times 4$ MHz. (c) Splitting of the ODMR spectra. (d) Width of the ODMR spectra. The red line are the fitting result from the simulated ODMR spectra (without light narrowing), while the blue line also considers the light narrowing effect [19].

equilibrium charge state of N-V centers under laser excitation can be obtained from the experimental data shown in Fig. 1(d). For the remaining N-V^- centers, we calculate their ODMR spectra using the method mentioned above. The laser power dependence of ODMR spitting and width are shown in Figs. 4(c) and 4(d).

By directly comparing the numerical (red) and experimental (black) results on laser power dependence, we find that the splitting values agree well from both sides. However, there is an obvious gap in the ODMR width values. This discrepancy may be mainly caused by the effect of light narrowing. As shown in Ref. [19], the width of ODMR spectra broadened by the microwave will be narrowed because the laser excitation effectively decreases the N-V spin relaxation time (T_1). To account for the effect of light narrowing, we rerun the above numerical simulation but without the effect of microwave power broadening. The obtained ODMR widths are treated as intrinsic widths (only the effects of N-V spin dephasing and charge neutralization are considered). Next, we use Eq. (1) from Ref. [19] to refine the dependence of the ODMR width on the laser power. This agrees well with the experimental results, as plotted by the blue symbols in Fig. 4(d).

III. DISCUSSION

The laser-induced charge neutralization of N-V^-–N^+ pairs would affect the performance of N-V–based quantum sensing. On the one hand, the fluorescence of N-V^0 increases the background level and decreases the spin-dependent fluorescent contrast of N-V^- centers. On the other hand, the influence on the splitting and linewidth can degrade the sensitivity based on ODMR detection, especially at low magnetic fields. Take the ODMR spectra shown in Figs. 4(a) and 4(b) as examples: when the laser intensity increases from 13 to 225 $\mu W/\mu m^2$, the ODMR contrast decreases from 0.036 to 0.026, the ODMR width narrows from 20.2 to 11.1 MHz and the N-V fluorescence counts increase from 170×10^3 counts/s to 2306×10^3 counts/s, resulting in an improvement of the magnetic sensitivity from 377 to 78 $\mu T/\sqrt{Hz}$. It is clear that higher laser intensity is preferred to increase the sensitivity of N-V–based quantum sensors in the weak excitation regime. For some applications where the laser intensity is limited by other factors, it is crucial to maintain a stable light power. For example, in experiments with living cells, the light exposure should be less than 20 J/cm^2 to avoid phototoxicity [12]. Assuming an experimental

integration time of 1 min and disregarding other factors (e.g., wavelength), the safe laser intensity is approximately 3.0 nW/μm^2. Therefore, it is necessary to maintain a stable laser power in biosensing applications of diamond N-V centers.

The contribution of internal electric fields becomes more significant at zero and low magnetic fields, so applications of N-V–based quantum sensors under these circumstances should pay particular attention to this effect. For example, zero-field magnetometry [41–43], zero- and ultralow-field nuclear magnetic resonance [44], magnetoneurography and magnetomyography [45], temperature sensing and intracellular sensing [18,46,47], and so on. Note that, although the light-induced charge-state conversion is a general effect, an external magnetic field could be applied to suppress the electric field coupling and mitigate the influence on magnetic sensitivity. We also measured the laser power dependence of ODMR width under an external magnetic field about 58 G. As shown in Fig. S6(c), only a slight narrowing effect has been observed, indicating a significant suppression on the coupling of the internal electric field by a large Zeeman splitting. It is worth noting that the dependence of ODMR splitting on laser intensity at (near) zero magnetic field cannot be explained by the light-narrowing effect alone.

In our numerical simulation, we made the simplified assumption that an N-V center pairs only with its nearest nitrogen atom. In fact, with multiple N atoms available, an N-V center could also pair with other nitrogen atoms. In addition, the pair "partner" of a particular N-V center may change over time. Nevertheless, the good agreement between the simulation and experimental results indicates that the simplified model captures the key features of laser-induced charge neutralization of N-V^-–N^+ pairs and the changes of local electric field environment.

In summary, we experimentally observe unambiguous laser-power dependence of (near) zero-field ODMR spectra of N-V ensembles in nano-, micro-, and bulk diamonds. In the weak-excitation regime, both the width and the splitting of the ODMR lines decrease with increasing laser power, which is accompanied by a reversible change of the height of the N-V^- ZPL peak. We use the N-V^-–N^+ pair model and perform numerical simulations to verify the effect of laser-induced charge neutralization. It turns out that both the laser power and the nitrogen-concentration dependence can be well understood with this simple model. These results will be useful in diamond-based quantum sensing applications, for example, probing biological intracellular signals and in studies of temperature-sensitive thin-film materials.

ACKNOWLEDGMENTS

The authors acknowledge helpful discussions with Neil Manson and Till Lenz. This work was supported by the Natural Science Foundation of Beijing, China (Grant No. Z200009), the National Key Research and Development Program of China (Grant No. 2019YFA0308100), the Chinese Academy of Sciences (Grants No. YJKYYQ2019 0082, No. XDB28030000, No. XDB33000000), and the National Natural Science Foundation of China (Grants No. 11974020, No. 12022509, No. 11934018, No. T2121001). Q.L. and R.-B.L. acknowledge the funding support from Hong Kong Research Grants Council - Collaborative Research Fund under Project No. C4007-19G. The work of D.B. was supported by the European Commission's Horizon Europe Framework Program under the Research and Innovation Action MUQUABIS GA Grant No. 101070546. The work of H.Z. was supported by Beijing Natural Science Foundation Grant No. L233021.

[1] A. Gruber, A. Drabenstedt, C. Tietz, L. Fleury, J. Wrachtrup, and C. V. Borczyskowski, Scanning confocal optical microscopy and magnetic resonance on single defect centers, Science **276**, 2012 (1997).

[2] G. Balasubramanian, I. Chan, R. Kolesov, M. Al-Hmoud, J. Tisler, C. Shin, C. Kim, A. Wojcik, P. R. Hemmer, and A. Krueger *et al.*, Nanoscale imaging magnetometry with diamond spins under ambient conditions, Nature **455**, 648 (2008).

[3] J. Maze, P. Stanwix, J. Hodges, S. Hong, J. Taylor, P. Cappellaro, L. Jiang, M. G. Dutt, E. Togan, and A. Zibrov *et al.*, Nanoscale magnetic sensing with an individual electronic spin in diamond, Nature **455**, 644 (2008).

[4] J. Taylor, P. Cappellaro, L. Childress, L. Jiang, D. Budker, P. Hemmer, A. Yacoby, R. Walsworth, and M. Lukin, High-sensitivity diamond magnetometer with nanoscale resolution, Nat. Phys. **4**, 810 (2008).

[5] V. M. Acosta, E. Bauch, M. P. Ledbetter, A. Waxman, L.-S. Bouchard, and D. Budker, Temperature dependence of the nitrogen-vacancy magnetic resonance in diamond, Phys. Rev. Lett. **104**, 070801 (2010).

[6] X.-D. Chen, C.-H. Dong, F.-W. Sun, C.-L. Zou, J.-M. Cui, Z.-F. Han, and G.-C. Guo, Temperature dependent energy level shifts of nitrogen-vacancy centers in diamond, Appl. Phys. Lett. **99**, 161903 (2011).

[7] M. W. Doherty, V. V. Struzhkin, D. A. Simpson, L. P. McGuinness, Y. Meng, A. Stacey, T. J. Karle, R. J. Hemley, N. B. Manson, and L. C. Hollenberg *et al.*, Electronic properties and metrology applications of the diamond NV^- center under pressure, Phys. Rev. Let. **112**, 047601 (2014).

[8] F. Dolde, H. Fedder, M. W. Doherty, T. Nöbauer, F. Rempp, G. Balasubramanian, T. Wolf, F. Reinhard, L. C. Hollenberg, and F. Jelezko *et al.*, Electric-field sensing using single diamond spins, Nat. Phys. **7**, 459 (2011).

[9] R. Schirhagl, K. Chang, M. Loretz, and C. L. Degen, Nitrogen-vacancy centers in diamond: Nanoscale sensors for physics and biology, Annu. Rev. Phys. Chem. **65**, 83 (2014).

[10] J.-H. Dai, Y.-X. Shang, Y.-H. Yu, Y. Xu, H. Yu, F. Hong, X.-H. Yu, X.-Y. Pan, and G.-Q. Liu, Optically detected magnetic resonance of diamond nitrogen-vacancy centers

under megabar pressures, Chin. Phys. Lett. **39**, 117601 (2022).
[11] P. J. Scheidegger, S. Diesch, M. L. Palm, and C. Degen, Scanning nitrogen-vacancy magnetometry down to 350 mK, Appl. Phys. Lett. **120**, 224001 (2022).
[12] P. P. Laissue, R. A. Alghamdi, P. Tomancak, E. G. Reynaud, and H. Shroff, Assessing phototoxicity in live fluorescence imaging, Nat. Methods **14**, 657 (2017).
[13] X. Feng, W.-H. Leong, K. Xia, C.-F. Liu, G.-Q. Liu, T. Rendler, J. Wrachtrup, R.-B. Liu, and Q. Li, Association of nanodiamond rotation dynamics with cell activities by translation-rotation tracking, Nano Lett. **21**, 3393 (2021).
[14] C. Grezes, B. Julsgaard, Y. Kubo, M. Stern, T. Umeda, J. Isoya, H. Sumiya, H. Abe, S. Onoda, T. Ohshima, V. Jacques, J. Esteve, D. Vion, D. Esteve, K. Mølmer, and P. Bertet, Multimode storage and retrieval of microwave fields in a spin ensemble, Phys. Rev. X **4**, 021049 (2014).
[15] S. E. Lillie, D. A. Broadway, N. Dontschuk, S. C. Scholten, B. C. Johnson, S. Wolf, S. Rachel, L. C. Hollenberg, and J.-P. Tetienne, Laser modulation of superconductivity in a cryogenic wide-field nitrogen-vacancy microscope, Nano Lett. **20**, 1855 (2020).
[16] V. M. Acosta, L. S. Bouchard, D. Budker, R. Folman, T. Lenz, P. Maletinsky, D. Rohner, Y. Schlussel, and L. Thiel, Color centers in diamond as novel probes of superconductivity, J. Supercond. Novel Magn. **32**, 85 (2019).
[17] Y. Schlussel, T. Lenz, D. Rohner, Y. Bar-Haim, L. Bougas, D. Groswasser, M. Kieschnick, E. Rozenberg, L. Thiel, and A. Waxman *et al.*, Wide-field imaging of superconductor vortices with electron spins in diamond, Phys. Rev. Appl. **10**, 034032 (2018).
[18] J. Choi, H. Zhou, R. Landig, H.-Y. Wu, X. Yu, S. E. Von Stetina, G. Kucsko, S. E. Mango, D. J. Needleman, and A. D. Samuel *et al.*, Probing and manipulating embryogenesis via nanoscale thermometry and temperature control, Proc. Natl. Acad. Sci. **117**, 14636 (2020).
[19] K. Jensen, V. M. Acosta, A. Jarmola, and D. Budker, Light narrowing of magnetic resonances in ensembles of nitrogen-vacancy centers in diamond, Phys. Rev. B **87**, 014115 (2013).
[20] N. Aslam, G. Waldherr, P. Neumann, F. Jelezko, and J. Wrachtrup, Photo-induced ionization dynamics of the nitrogen vacancy defect in diamond investigated by single-shot charge state detection, New J. Phys. **15**, 013064 (2013).
[21] T. Mittiga, S. Hsieh, C. Zu, B. Kobrin, F. Machado, P. Bhattacharyya, N. Rui, A. Jarmola, S. Choi, and D. Budker *et al.*, Imaging the local charge environment of nitrogen-vacancy centers in diamond, Phys. Rev. Lett. **121**, 246402 (2018).
[22] N. B. Manson, M. Hedges, M. S. Barson, R. Ahlefeldt, M. W. Doherty, H. Abe, T. Ohshima, and M. J. Sellars, NV^{-}–N^{+} pair centre in 1b diamond, New J. Phys **20**, 113037 (2018).
[23] S. Baier, C. E. Bradley, T. Middelburg, V. V. Dobrovitski, T. H. Taminiau, and R. Hanson, Orbital and spin dynamics of single neutrally-charged nitrogen-vacancy centers in diamond, Phys. Rev. Lett. **125**, 193601 (2020).
[24] S. Dhomkar, H. Jayakumar, P. R. Zangara, and C. A. Meriles, Charge dynamics in near-surface, variable-density ensembles of nitrogen-vacancy centers in diamond, Nano Lett. **18**, 4046 (2018).
[25] C. Shinei, M. Miyakawa, S. Ishii, S. Saiki, S. Onoda, T. Taniguchi, T. Ohshima, and T. Teraji, Equilibrium charge state of NV centers in diamond, Appl. Phys. Lett. **119**, 254001 (2021).
[26] I. C. Barbosa, J. Gutsche, and A. Widera, Impact of charge conversion on NV-center relaxometry, arXiv preprint ArXiv:2301.01063.
[27] S. Ito, M. Tsukamoto, K. Ogawa, T. Teraji, K. Sasaki, and K. Kobayashi, Optical-power-dependent splitting of magnetic resonance in nitrogen-vacancy centers in diamond, J. Phys. Soc. Jpn. **92**, 084701 (2023).
[28] See Supplemental Material http://link.aps.org/supplemental/10.1103/PhysRevApplied.21.044051 for details of the system, the experimental and theoretical methods, and the supplemental data of the hybrid sensors, which includes Refs. [29–38].
[29] E. Van Oort and M. Glasbeek, Electric-field-induced modulation of spin echoes of NV centers in diamond, Chem. Phys. Lett. **168**, 529 (1990).
[30] S. Whitehead and W. Hackett, Measurement of the specific inductive capacity of diamonds by the method of mixtures, Proc. Phys. Soc. (1926-1948) **51**, 173 (1939).
[31] X.-D. Chen, S. Li, A. Shen, Y. Dong, C.-H. Dong, G.-C. Guo, and F.-W. Sun, Near-infrared-enhanced charge-state conversion for low-power optical nanoscopy with nitrogen-vacancy centers in diamond, Phys. Rev. Appl. **7**, 014008 (2017).
[32] Z. Yuan, M. Fitzpatrick, L. V. Rodgers, S. Sangtawesin, S. Srinivasan, and N. P. De Leon, Charge state dynamics and optically detected electron spin resonance contrast of shallow nitrogen-vacancy centers in diamond, Phys. Rev. Res. **2**, 033263 (2020).
[33] P. Siyushev, H. Pinto, M. Vörös, A. Gali, F. Jelezko, and J. Wrachtrup, Optically controlled switching of the charge state of a single nitrogen-vacancy center in diamond at cryogenic temperatures, Phys. Rev. Lett. **110**, 167402 (2013).
[34] S. A. Savinov, V. V. Sychev, and D. Bi, Diamond nitrogen-vacancy center charge state ratio determination at a given sample point, J. Lumin. **248**, 118981 (2022).
[35] R. P. Roberts, M. L. Juan, and G. Molina-Terriza, Spin-dependent charge state interconversion of nitrogen vacancy centers in nanodiamonds, Phys. Rev. B **99**, 174307 (2019).
[36] R. Giri, C. Dorigoni, S. Tambalo, F. Gorrini, and A. Bifone, Selective measurement of charge dynamics in an ensemble of nitrogen-vacancy centers in nanodiamond and bulk diamond, Phys. Rev. B **99**, 155426 (2019).
[37] G. Lindblad, On the generators of quantum dynamical semigroups, Commun. Math. Phys. **48**, 119 (1976).
[38] S. M. Tan, A computational toolbox for quantum and atomic optics, J. Opt. B: Quantum Semiclass. Opt. **1**, 424 (1999).
[39] A. M. Ferrari, K. E. El-Kelany, F. S. Gentile, M. D'Amore, and R. Dovesi, The NV^{-} N^{+} charged pair in diamond: A quantum-mechanical investigation, Phys. Chem. Chem. Phys. **23**, 18724 (2021).
[40] R. Löfgren, S. Öberg, and J. Larsson, A theoretical study of de-charging excitations of the NV-center in diamond involving a nitrogen donor, New J. Phys. **22**, 123042 (2020).

[41] H. Zheng, J. Xu, G. Z. Iwata, T. Lenz, J. Michl, B. Yavkin, K. Nakamura, H. Sumiya, T. Ohshima, J. Isoya, J. Wrachtrup, A. Wickenbrock, and D. Budker, Zero-field magnetometry based on nitrogen-vacancy ensembles in diamond, Phys. Rev. Appl. **11**, 064068 (2019).

[42] P. J. Vetter, A. Marshall, G. T. Genov, T. F. Weiss, N. Striegler, E. F. Großmann, S. Oviedo-Casado, J. Cerrillo, J. Prior, P. Neumann, and F. Jelezko, Zero- and low-field sensing with nitrogen-vacancy centers, Phys. Rev. Appl. **17**, 044028 (2022).

[43] N. Wang, C.-F. Liu, J.-W. Fan, X. Feng, W.-H. Leong, A. Finkler, A. Denisenko, J. Wrachtrup, Q. Li, and R.-B. Liu, Zero-field magnetometry using hyperfine-biased nitrogen-vacancy centers near diamond surfaces, Phys. Rev. Res. **4**, 013098 (2022).

[44] D. Budker, Extreme nuclear magnetic resonance: Zero field, single spins, dark matter . . ., J. Magn. Reson. **306**, 66 (2019).

[45] C. Zhang, J. Zhang, M. Widmann, M. Benke, M. Kübler, D. Dasari, T. Klotz, L. Gizzi, O. Röhrle, and P. Brenner *et al.*, Optimizing NV magnetometry for magnetoneurography and magnetomyography applications, Front. Neurosci. **16**, 1034391 (2023).

[46] G. Kucsko, P. C. Maurer, N. Y. Yao, M. Kubo, H. J. Noh, P. K. Lo, H. Park, and M. D. Lukin, Nanometre-scale thermometry in a living cell, Nature **500**, 54 (2013).

[47] M. Fujiwara, S. Sun, A. Dohms, Y. Nishimura, K. Suto, Y. Takezawa, K. Oshimi, L. Zhao, N. Sadzak, and Y. Umehara *et al.*, Real-time nanodiamond thermometry probing in vivo thermogenic responses, Sci. Adv. **6**, eaba9636 (2020).